Efficient Charge Injection in Organic Field-Effect Transistors Enabled by Low-Temperature Atomic Layer Deposition of Ultrathin VO_x Interlayer

*Yuanhong Gao, Youdong Shao, Lijia Yan, Hao Li, Yantao Su, Hong Meng, and Xinwei Wang**

Charge injection at metal/organic interface is a critical issue for organic electronic devices in general as poor charge injection would cause high contact resistance and severely limit the performance of organic devices. In this work, a new approach is presented to enhance the charge injection by using atomic layer deposition (ALD) to prepare an ultrathin vanadium oxide (VO_x) layer as an efficient hole injection interlayer for organic field-effect transistors (OFETs). Since organic materials are generally delicate, a gentle low-temperature ALD process is necessary for compatibility. Therefore, a new low-temperature ALD process is developed for VO_x at 50 °C using a highly volatile vanadium precursor of tetrakis(dimethylamino)vanadium and non-oxidizing water as the oxygen source. The process is able to prepare highly smooth, uniform, and conformal VO_x thin films with precise control of film thickness. With this ALD process, it is further demonstrated that the ALD VO_x interlayer is able to remarkably reduce the interface contact resistance, and, therefore, significantly enhance the device performance of OFETs. Multiple combinations of the metal/VO_x/organic interface (i.e., Cu/VO_x/pentacene, Au/VO_x/pentacene, and Au/VO_x/BOPAnt) are examined, and the results uniformly show the effectiveness of reducing the contact resistance in all cases, which, therefore, highlights the broad promise of this ALD approach for organic devices applications in general.

1. Introduction

Organic electronic devices have recently attracted great attention for their high mechanical flexibility and low fabrication cost with a huge variety of materials choices for fine-tuning the device properties,[1] and they have been used in many important applications, such as active-matrix displays,[2] radiofrequency identification tags,[3] pressure sensors,[4] and complementary integrated circuits.[5,6] However, a critical issue for organic devices in general is the contact resistance at their metal/organic interfaces.[7] Compared to inorganic devices, the contact resistance for organic devices is normally fairly large, which can severely impede the charge injection at the contacts, and, therefore, limit the effective carrier mobility, the device switching speed, and the saturated output current for organic field-effect transistors (OFETs).[8] High contact resistance could also hinder the downscaling of the channel length for OFETs, and would therefore result in difficulty for high-frequency applications.[8,9] The contact issue is much more pronounced for p-type OFETs, where a high work function metal is normally needed to match with the low-lying HOMO level (or valence band) of the semiconducting organic material. On the other hand, high work function metals (e.g., Au[10]) are generally highly polarizable,[11] and, therefore, they are highly affected by the interfacial dipole formed at the metal/organic contact, which usually considerably lowers the metal work function, misaligns the energy levels, and creates an injection barrier for holes at the interface.[11] Therefore, engineering the metal/organic interface becomes an important task for enhancing the performance of organic devices.[7]

Recently, inserting a nm-thick layer of metal oxide at the metal/organic interface has been suggested effective to facilitate the hole injection and reduce the interface contact resistance.[12–14] A particularly important example for the oxide is vanadium pentoxide (V_2O_5).[15] V_2O_5 has a high electron affinity of −6.7 eV with a large work function of −7.0 eV,[16] which is suitable for injecting holes in organic devices.[17–19] However, although many fabrication methods of V_2O_5 films have been reported,[20–25] preparing a suitable V_2O_5 layer directly on organic materials is still a big challenge, which seriously limits its application for top-contact OFET devices. The most critical issue with the fabrication method is its compatibility with organic materials. Organic materials are generally delicate; they can be severely degraded at high temperature or under oxidizing ambient, which therefore precludes many high-temperature processes as well as those processes using strongly oxidizing agents, such as O_3 and oxygen plasma. Sputtering

Y. Gao, Dr. Y. Shao, L. Yan, H. Li, Dr. Y. Su, Prof. H. Meng, Prof. X. Wang
School of Advanced Materials
Shenzhen Graduate School
Peking University
Shenzhen 518055, P.R. China
E-mail: wangxw@pkusz.edu.cn

DOI: 10.1002/adfm.201600482

© 2016 WILEY-VCH Verlag GmbH & Co. KGaA, Weinheim

and evaporation should also be cautioned, since the highly energetic atoms from the oxide source could also damage the substrate organic materials. Caution should also be taken for solution-based processes, since the solvent may dissolve or interact with the organic materials. On the other hand, the quality of the prepared V_2O_5 films is also critical for device performance. As the thickness of the V_2O_5 interlayer is only a few nanometers, one needs a preparation method that has precise controllability in film thickness. Also, since crystalline organic semiconductor usually has a terrace-structured surface,[26] the prepared V_2O_5 layer should be able to uniformly and conformally cover the surface terrace. Additionally, in order for future industrial scale-up, good large-area uniformity of the V_2O_5 layer should be highly preferred.

Atomic layer deposition (ALD) is a promising approach to fabricate high-quality vanadium oxide (VO_x) thin films for this purpose, as ALD offers angstrom-precision control of film thickness with excellent film conformality and uniformity via the employment of self-limiting surface chemistry reactions in an alternate manner.[27,28] Unfortunately, the currently existing ALD processes for VO_x either need relatively high process temperature[29–31] or use strongly oxidizing agents,[21,32–35] which are not suitable for the deposition on delicate organic materials. Thus, developing a new VO_x ALD process with gentle deposition conditions of using non-oxidizing agents at low process temperature is greatly in need.

In this work, we report a new low-temperature ALD process for VO_x with very gentle deposition conditions. The process used a highly volatile vanadium precursor of tetrakis(dimethylamino) vanadium ($V(dma)_4$), along with a non-oxidizing agent of H_2O vapor as the oxygen source. Since $V(dma)_4$ is highly reactive with H_2O, the ALD reactions were able to proceed at a fairly low temperature of 50 °C. The deposited VO_x films were very good in uniformity, smoothness, and conformality, and the film thickness could be precisely controlled at an angstrom level. With this gentle low-temperature ALD process, high-quality ultrathin VO_x films could be safely deposited on delicate organic materials, which enabled us to employ ALD, for the first time, to prepare the charge injection layer directly on organic materials. As later shown in this work, the ALD-prepared VO_x interlayer exhibited excellent hole injection behavior with significantly reduced contact resistance at the metal/organic interface. To demonstrate the general applicability of this approach, we employed three exemplary metal/organic combinations, with two types of organic semiconducting materials (i.e., pentacene and 2,6-bis(4-methoxyphenyl)anthracene) and two types of contact metals (i.e., Au and Cu). Our results clearly showed that the ALD VO_x interlayer was highly effective for reducing the contact resistance in all these cases, which highlighted the broad promise of this ALD approach for general organic electronics applications.

2. Results and Discussion

Low-temperature ALD of VO_x was carried out in a home-built ALD reactor by using $V(dma)_4$ as the vanadium precursor and H_2O vapor as the oxygen source. $V(dma)_4$ and H_2O were both kept at room temperature, and their vapors were alternately delivered into the reactor chamber during the ALD process. To ensure the sufficient delivery of the vanadium precursor, high-pressure N_2 gas was used to assist the delivery of $V(dma)_4$ vapor. Since organic materials are generally delicate, a low deposition temperature of 50 °C was particularly chosen for minimizing the potential thermal effect on organic materials. On the other hand, the desorption of physisorbed H_2O is rather slow at 50 °C, thus a particularly long purge time of 100 s was employed to remove the excess unreacted H_2O vapor. To investigate the saturation growth behavior of VO_x, multiple doses for H_2O or $V(dma)_4$ were used in each of their half cycles. Typical ALD saturation growth behavior is demonstrated in **Figure 1**a,b. With increasing the dose number for H_2O (or $V(dma)_4$) while keeping fixed single dose for $V(dma)_4$ (or H_2O), the film growth rate remained fairly constant at ≈0.30 Å cycle^{-1}, which clearly indicated that the surface chemistry involved in this ALD process was indeed self-limiting. The results also showed that single precursor doses were sufficient to saturate the surface reactions (equivalent exposures for single doses of $V(dma)_4$ and H_2O were roughly 0.02 and 0.05 Torr s, respectively). Therefore, we used only single doses for both $V(dma)_4$ and H_2O in the following deposition experiments. Linear growth behavior was further examined by varying the total number of ALD cycles. As shown in Figure 1c, the film thickness followed a good linear relation with the total cycle number, suggesting that the film thickness can be precisely controlled by digitally varying the total ALD cycles.

The as-deposited VO_x films were amorphous (no peak in XRD spectrum), and the film composition was analyzed by Rutherford backscattering spectrometry (RBS). As the RBS spectrum shown in Figure 1d, the O/V atomic ratio (i.e., x) of VO_x was determined as 2.42 ± 0.03. Notice that V in $V(dma)_4$ is four-fold coordinated, and thus VO_2 (i.e., $x = 2$) would be expected if the surface reaction followed simple and complete ligand exchange between $V(dma)_4$ and H_2O. The finding that the films contained extra oxygen ($x > 2$) suggested that the films might contain additional hydroxyl groups and/or be oxidized after exposed to air. X-ray photoelectron spectroscopy (XPS) was further employed to analyze the films. XPS was performed on an as-deposited 30 nm VO_x film, and the resultant high-resolution spectrum was shown in Figure 1e, where the peak of V $2p_{3/2}$ located near 517.3 eV. Deconvolution of the V $2p_{3/2}$ peak revealed that the majority of V was in +5 state (the corresponding binding energies for V^{5+} and V^{4+} were 517.4 and 516.2 eV, respectively),[36] suggesting that the oxidation of the deposited VO_x films occurred immediately after exposed to air. In fact, the majority vanadium in +5 state should be beneficial for the charge injection performance of VO_x, as V_2O_5 (with V^{4+} defects) was actually referred as a good hole injection material.[16]

XPS was also used to evaluate the film purity. The sample was first treated with Ar^+ sputtering for 60 s to remove the surface adventitious carbon. The obtained XPS survey spectrum was shown in Figure 1f, where the deposited VO_x film was found to be quite good in purity, with only 1.3 at% for N impurity and no detectable C impurity (i.e., below the detection limit of ≈1 at.%). The deposited VO_x films were quite smooth. As examined by atomic force microscopy (AFM), the rms roughness for a ≈10 nm film was only 0.32 nm (Figure 1g), which increased only slightly as compared to the roughness of the underneath

© 2016 WILEY-VCH Verlag GmbH & Co. KGaA, Weinheim

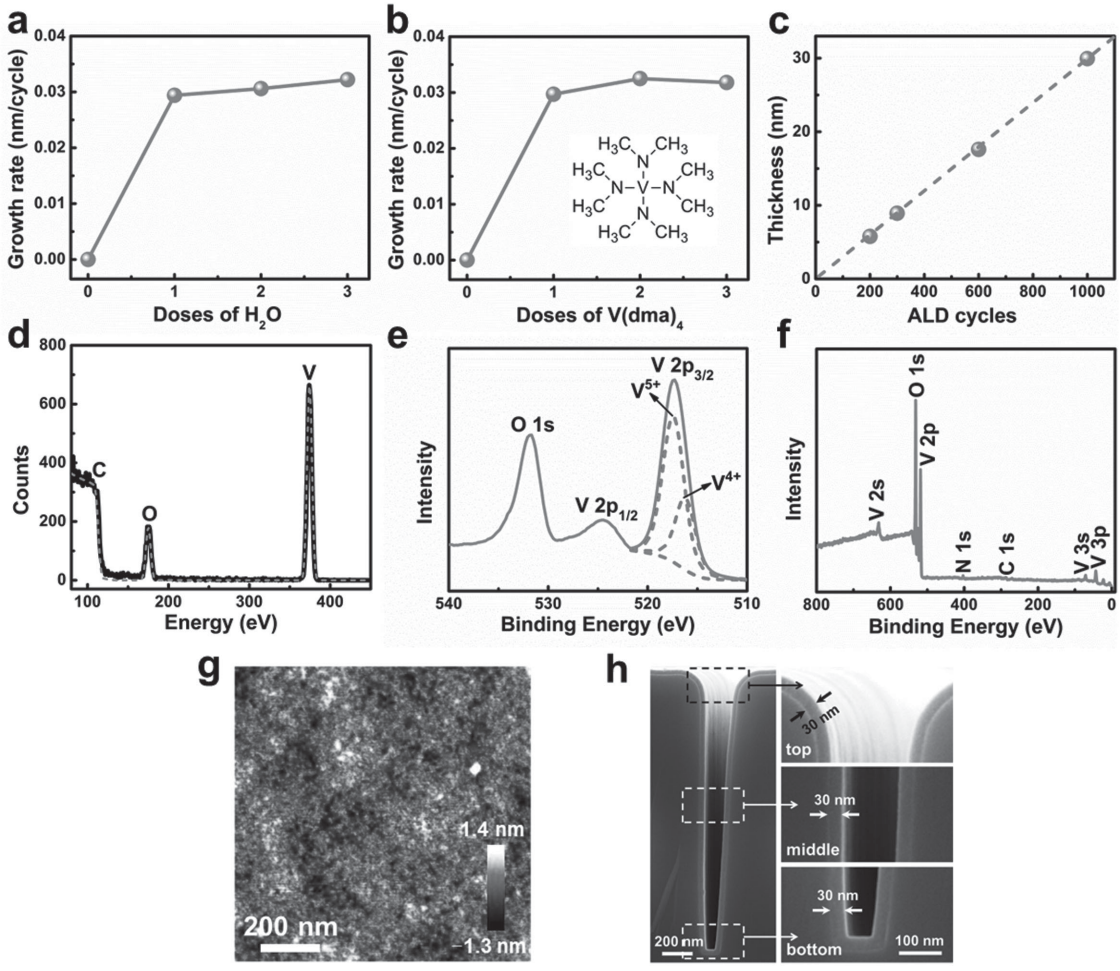

Figure 1. Data plotted in panels (a) and (b) showing that the ALD growth rate of VO_x approaches a constant value as the precursor dosage increases. a) Growth rate with respect to the number of H_2O doses while keeping fixed single dose for $V(dma)_4$. b) Growth rate with respect to the number of $V(dma)_4$ doses while keeping fixed single dose for H_2O. c) Film thickness as a function of total ALD cycles. d) RBS spectrum (black) with a simulated spectrum (grey, dashed) for a ≈30 nm VO_x film deposited on glassy carbon. e) High-resolution XPS showing V 2p and O 1s peaks for ALD VO_x. f) XPS survey spectrum for the VO_x film with 60 s Ar^+ sputtering to remove the surface adventitious carbon. g) AFM image of a ≈10 nm VO_x film showing an rms roughness of only 0.32 nm. h) Cross-sectional SEM image showing that VO_x was conformally deposited (1000 cycles) inside a deep narrow trench with aspect ratio as high as 10:1. The deposition temperature was 50 °C for all these experiments.

thermal oxide substrate (i.e., 0.29 nm, see Figure S1, Supporting Information). Conformal coating of this ALD process was further evaluated by depositing VO_x films into deep narrow trenches with high aspect ratios. As shown in Figure 1h, for a trench with 10:1 aspect ratio, the VO_x film prepared by our ALD process was able to conformally cover the trench with uniform thickness throughout the entire trench, which clearly demonstrated the excellent conformality of this ALD process.

So far, we have presented a well-behaved low-temperature ALD process for VO_x. The process followed typical layer-by-layer ALD growth fashion, and was able to deposit pure, smooth, and conformal VO_x thin films with highly controllable film thickness. In the following, we will apply this ALD process to prepare ultrathin VO_x interlayers for improving the charge injection at metal/organic interface in OFETs. To show its generality, we will demonstrate the applicability of this ALD approach for two types of organic semiconductor materials (i.e., a widely used material of pentacene and a newly developed material of 2,6-bis(4-methoxyphenyl)anthracene (BOPAnt)[37]) along with two types of contact metals (i.e., Au and Cu).

Before making the OFET devices, the compatibility of this ALD process with the organic materials was first examined. We deposited VO_x on thermally evaporated 100 nm pentacene films at 50 °C with various total ALD cycles, and performed XPS on these VO_x-coated samples. As shown in **Figure 2**a, the obtained XPS spectra confirmed that VO_x was indeed deposited on top of the pentacene surface. AFM was further employed to examine the morphological change after ALD. As compared in Figure 2b,c, no morphological change was observed, and the terrace structure of the crystalline pentacene films was well maintained, showing that the original pentacene was well preserved after the conformal ALD coating of VO_x. Similar results were also obtained for the other organic material of BOPAnt (Figure S2, Supporting Information), which demonstrated that the gentle low-temperature ALD process developed in this work was generally suitable for processing on delicate organic materials.

© 2016 WILEY-VCH Verlag GmbH & Co. KGaA, Weinheim

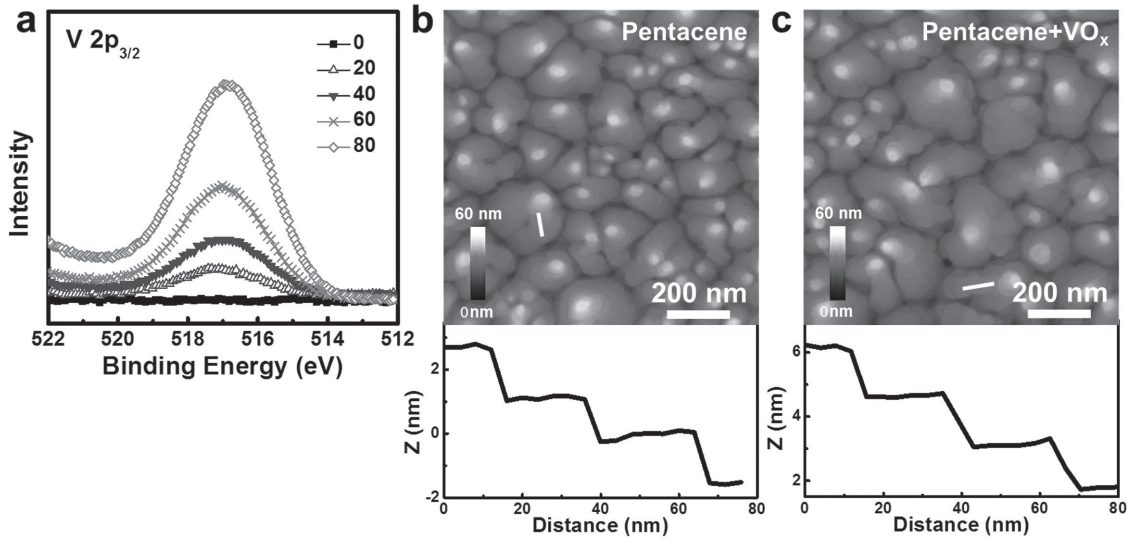

Figure 2. a) XPS spectra for VO_x/pentacene samples confirming the presence of V on pentacene surface, and the V peak intensity followed an increasing trend with the total ALD cycle number. Comparison of the AFM images for b) pentacene and c) VO_x/pentacene with 40 ALD cycles, showing no morphological change after ALD. Bottom profiles present the height traces of the line sections labeled in the AFM images, respectively.

To demonstrate the enhanced charge injection with the addition of the VO_x interlayer, we fabricated bottom-gate/top-contact OFET devices as schematically illustrated in **Figure 3**a. ≈70 nm organic semiconductor material of pentacene or BOPAnt was first thermally evaporated on SiO_2/p^+-Si substrate. Then, ALD of ultrathin VO_x was performed on top of the organic layer, which was followed by thermal evaporation of ≈50 nm source/drain contact metal. The thickness of the VO_x interlayer was systematically varied by setting different total ALD cycles.

As a first example, we used a widely used organic material of pentacene for the semiconductor layer, and a relatively cheap metal of Cu for the source/drain metal contacts. Typical output and transfer characteristics of these Cu/VO_x/pentacene OFETs are shown in Figure 3b–g. With the addition of the VO_x layer, the output current was significantly increased, and, in particular, 40 cycles of ALD VO_x (≈1 nm) gave out the highest saturated drain current (I_D), which was almost 3 times higher than that for the device without the VO_x layer (i.e., 0 cycles). Meanwhile, as expected, the off-state current was not affected by inserting the VO_x layer (Figure 3g), so the high I_{on}/I_{off} ratio over 10^5 was maintained (Table S2, Supporting Information). Field-effect carrier mobility (μ_{FE}) was further extracted in the saturated region (V_D = −60 V), using the relation $I_D = \frac{W}{2L}\mu_{FE}C_i(V_G - V_T)^2$, where I_D is the saturated drain current, V_G is the gate voltage, and W, L, V_T, and C_i are the channel width, channel length, threshold voltage, and the areal capacitance of the gate insulator, respectively. As the data plotted in Figure 3h, μ_{FE} also showed significant increase by adding the VO_x interlayer, with the highest μ_{FE} of 0.80 $cm^2\ V^{-1}\ s^{-1}$ (for 40-cycle VO_x), as compared to 0.29 $cm^2\ V^{-1}\ s^{-1}$ for the devices without VO_x. Notice that μ_{FE} is an apparent (effective) quantity that takes into account not only the material intrinsic mobility but also the effects from the contacts.[38] To separately study the contact effects, we used Y function method (YFM) to extract the contact resistance (R_c, normalized by channel width).[9] YFM utilizes the device transfer characteristics in the linear region, and is able to give out the value of R_c for each individual OFET device.[38] YFM can also give out the low-field mobility (μ_0), which is regarded as the intrinsic carrier mobility, corresponding to the maximum achievable mobility for the transistors when R_c is completely diminished.[39] The extracted R_c were plotted in Figure 3h, where a clear reduction of the contact resistance from 64 kΩ cm to only 10 kΩ cm was observed for 40 cycles of ALD VO_x. These results confirmed that the contact resistance was indeed reduced by ALD VO_x, which, therefore, greatly enhanced the device performance. Notice that the low-field mobility (μ_0) (also plotted in Figure 3h) was almost a constant (≈0.87 $cm^2\ V^{-1}\ s^{-1}$) with respect to the ALD cycles, which indicated that the intrinsic mobility property of pentacene was well maintained after ALD, although we also observed an increased onset voltage, which might be caused by oxygen doping of pentacene during the process.[40,41]

To further demonstrate the generality of this ALD VO_x approach, we also replaced the contact metal with Au, and fabricated Au/VO_x/pentacene OFETs with the same device structure (Figure 3a). Representative device characteristics were shown in **Figure 4**a–c (also see Figure S4, Supporting Information), where very similar results as Cu/VO_x/pentacene were obtained for Au/VO_x/pentacene OFETs. Given a fixed V_G at −60 V, the saturated drain current was greatly increased by adding the ALD VO_x interlayer, with the highest drain current obtained for the 40-cycle ALD case. 40 cycles of ALD VO_x was also able to significantly reduce the Au/pentacene contact resistance from 103 to 15 kΩ cm (Figure 4c), which greatly enhanced the field-effect mobility (μ_{FE}) from 0.27 to 0.70 $cm^2\ V^{-1}\ s^{-1}$. In addition, as expected, the extracted low-field mobility (μ_0) was also a constant for all these devices.

Moreover, we also used BOPAnt, a different type of organic semiconductor material, to examine the effectiveness of this ALD VO_x approach. Au/VO_x/BOPAnt OFETs were also fabricated with the same bottom-gate/top-contact configuration

© 2016 WILEY-VCH Verlag GmbH & Co. KGaA, Weinheim

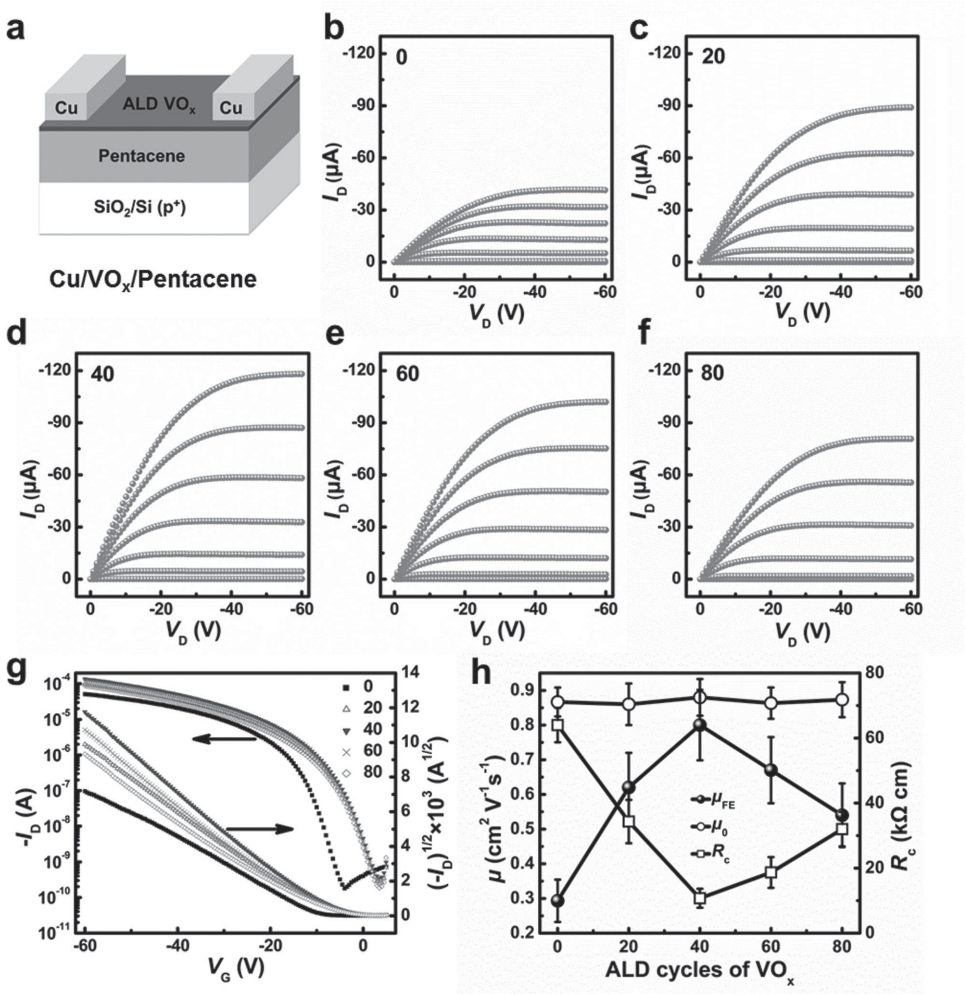

Figure 3. a) Schematic illustration of the bottom-gate/top-contact structure of the Cu/VO_x/pentacene OFET device. Output characteristics of Cu/VO_x/pentacene OFETs b) without VO_x (i.e., 0 cycles) and with c) 20, d) 40, e) 60, or f) 80 ALD cycles of VO_x, where V_G was varied from 0 to −60 V, in steps of −10 V. g) Comparison of the associated transfer characteristics (V_D = −60 V). h) Variation of the field-effect mobility (μ_{FE}) obtained in the saturation region (V_D = −60 V), and the low-field mobility (μ_0) and contact resistance (R_c) extracted by YFM.

(Figure 3a), and the corresponding device characteristics were shown in Figure 4d–f (also see Figure S5, Supporting Information). Similar trend for the ALD VO_x interlayer was again shown. With 20 cycles of ALD VO_x, the Au/BOPAnt contact resistance was significantly reduced from 71 down to 10 kΩ cm, which appreciably boosted the field-effect mobility (μ_{FE}) from 1.09 to 1.56 $cm^2\ V^{-1}\ s^{-1}$. In fact, in this Au/BOPAnt combination, pronounced super-linear behavior for I_D was shown in the linear region, which suggested that the contact resistance was quite a critical issue in this case.[19] As shown in Figure S5 (Supporting Information), our data clearly showed that this super-linear behavior could be completely removed by inserting a 20-cycle ALD VO_x layer, which again corroborated the effectiveness of reducing the contact resistance by this ALD VO_x approach.

To understand the VO_x effect, we measured the work functions of the VO_x-coated Cu electrodes by Kelvin probe method,[42] since the contact resistance is closely related to the mismatch between the electrode Fermi level (work function) and the HOMO level of the (p-type) organic molecules.[38] If the electrode Fermi level is much higher than the organic HOMO level (after taking into account the effect from interfacial dipole[43]), a large barrier for injecting holes would be formed at the interface, which would resulted in a large contact resistance. The measured work function of VO_x-coated Cu (i.e., Cu/VO_x) was plotted, in **Figure 5**, with respect to the ALD cycles of VO_x. The work function showed a monotonously increasing trend (in magnitude) with the thickness of the VO_x interlayer, with particularly steep increase for the first 40 ALD cycles. This trend clearly demonstrated the effectiveness of VO_x for increasing the electrode effective work function, and which, therefore, explained the appreciable reduction of the contact resistance for the first 40 ALD cycles (≈1 nm) of VO_x. On the other hand, further increasing the VO_x thickness (≥60 cycles) showed only little effect on the work function, and also, since ALD VO_x was found highly resistive (≈10^5 Ω cm, by two-probe measurement), the resistance across the VO_x interlayer would dominate the total contact resistance if VO_x was too thick. Consequently, as experimentally observed, further increasing the total ALD cycles above 40 actually resulted in an increase of the contact resistance for the Cu/pentacene interface.

© 2016 WILEY-VCH Verlag GmbH & Co. KGaA, Weinheim

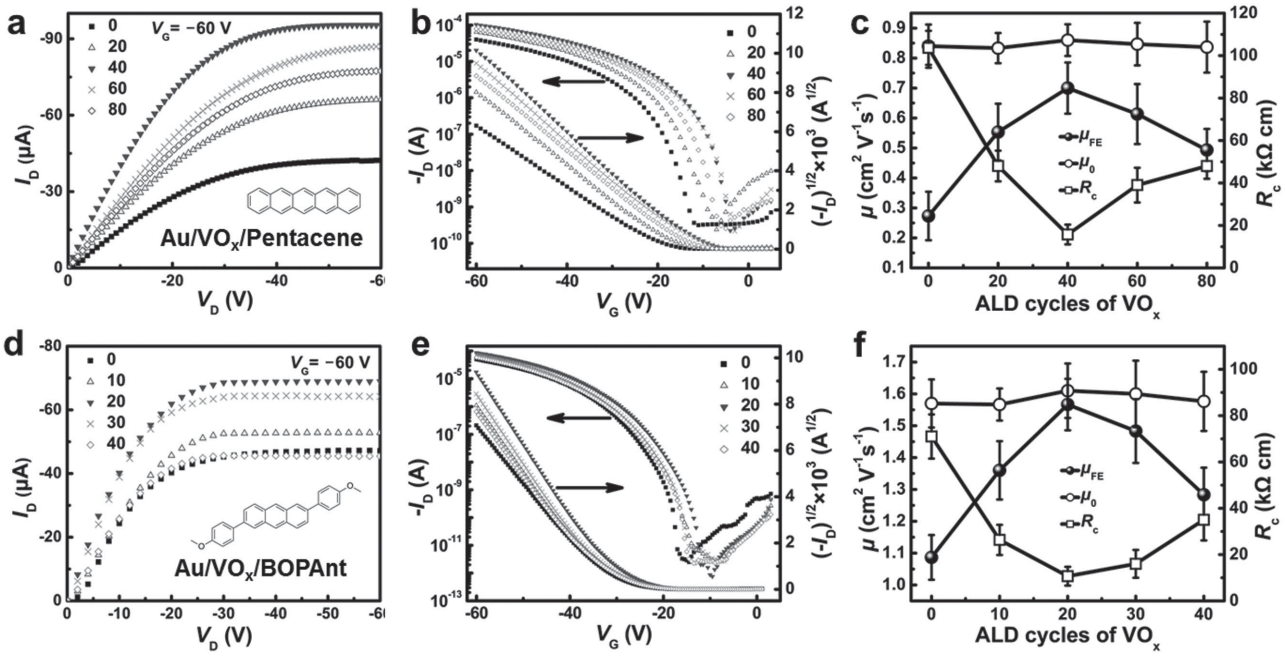

Figure 4. a) Output and b) transfer characteristics of Au/VO_x/pentacene OFETs with various VO_x thickness (i.e., 0, 20, 40, 60, and 80 ALD cycles), and c) the corresponding μ_{FE}, μ_0, and R_c. d) Output and e) transfer characteristics of Au/VO_x/BOPAnt OFETs with various VO_x thickness (i.e., 0, 10, 20, 30, and 40 ALD cycles), and f) the corresponding μ_{FE}, μ_0, and R_c. Note that the output characteristics are only shown for $V_G = -60$ V in panels (a) and (d); see Figures S4 and S5 (Supporting Information) for other V_G's. The μ_{FE}, μ_0, and R_c in panels (c) and (f) were obtained by the same method as previous (Figure 3h), respectively.

In addition, we also examined the shelf lifetime of these ALD VO_x-treated OFETs. Organic devices normally suffer from severe moisture/oxygen degradation. ALD Al_2O_3 is a well-known barrier for moisture/oxygen transmission,[44] and, thus, it has been used to encapsulate the organic devices for protection.[45,46] As ALD films are generally uniform and compact, we expected that our ALD VO_x films, although very thin, should also protect, at least to some extent, the devices from moisture/oxygen degradation. In fact, we found that this protection effect was quite pronounced, even though the thickness of ALD VO_x was just a couple of nanometers. As shown in **Figure 6**, all three types of the OFETs (i.e., Cu/VO_x/pentacene, Au/VO_x/pentacene, and Au/VO_x/BOPAnt) exhibited much enhanced performance retention (in normalized μ_{FE}, also see Figure S6 in the Supporting Information for μ_0 and R_c) for the ALD VO_x-treated devices, with thicker VO_x layer showing better retention in μ_{FE}. These results indicated that ALD VO_x was also a good barrier material for moisture/oxygen transmission. In fact, as we have found the optimal thickness for ALD VO_x as the hole injection interlayer, we could deposit an additional ALD layer of Al_2O_3 for the encapsulation purpose. To implement this idea, 300 cycles of ALD Al_2O_3 (≈30 nm) was additionally deposited after the completion of the whole OFET devices (i.e., after source/drain metal evaporation) with optimized VO_x thicknesses respectively for Cu/VO_x/pentacene, Au/VO_x/pentacene, and Au/VO_x/BOPAnt OFETs. As the data shown in Figure 6, this combined dual-ALD approach was able to provide an excellent performance retention with over 83% retention of the device field-effect mobility (μ_{FE}) for all these OFETs, which clearly demonstrated the effectiveness of this combined ALD approach.

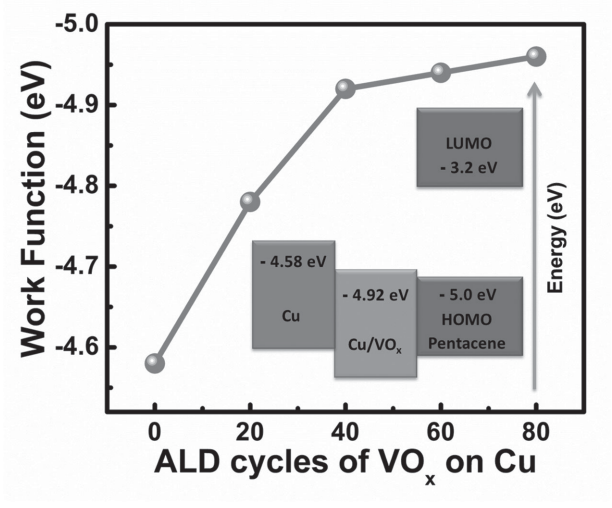

Figure 5. Work function of ALD VO_x-coated Cu, showing an increasing trend for the work function (in magnitude) with respect to the VO_x cycles. Inset: schematic illustration of the energy level alignment for the Cu/VO_x/pentacene interface.

3. Conclusion

In this work, we presented a new approach of using ALD to prepare high-quality ultrathin VO_x film as a hole injection layer for OFETs. In order to be compatible with delicate organic

© 2016 WILEY-VCH Verlag GmbH & Co. KGaA, Weinheim

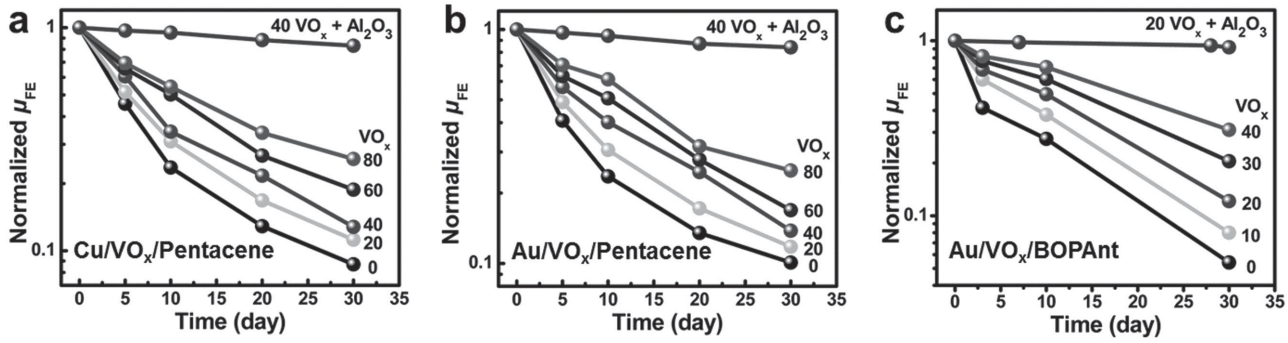

Figure 6. Normalized field-effect mobility (μ_{FE}) as a function of shelf time for a) Cu/VO_x/pentacene, b) Au/VO_x/pentacene, and c) Au/VO_x/BOPAnt OFETs, respectively.

materials, a new VO_x ALD process with gentle processing conditions of using low deposition temperature of 50 °C with non-oxidizing H_2O as the oxygen source was particularly developed. The process also used a highly volatile and reactive compound of tetrakis(dimethylamino)vanadium as the vanadium source. The process is able to prepare highly smooth and uniform VO_x thin films with precise control of film thickness. The deposited VO_x films were also able to uniformly and conformally cover the terrace structure on the surface of organic materials without causing apparent damage, which therefore demonstrated the compatibility of this ALD process for organic devices. With this low-temperature ALD process, we further demonstrated that the ALD VO_x hole injection layer was able to remarkably reduce the contact resistance at the metal/organic interface, and, therefore, significantly enhanced the device performance of OFETs (e.g., μ_{FE}). Multiple combinations of the metal/VO_x/organic interface (i.e., Cu/VO_x/pentacene, Au/VO_x/pentacene, and Au/VO_x/BOPAnt) were examined, and the results uniformly showed the effectiveness of reducing the contact resistance in all cases, which therefore highlighted the broad promise of this ALD approach for organic devices applications in general.

4. Experimental Section

Atomic Layer Deposition of VO_x: VO_x thin films were deposited in a home-built tubular ALD reactor at 50 °C. $V(dma)_4$ and H_2O vapor were used as the vanadium precursor and oxygen source, respectively. Both of $V(dma)_4$ and H_2O were kept at room temperature in glass containers, respectively. During the deposition, $V(dma)_4$ was delivered into the deposition chamber with the assist of purified N_2 gas (through a Gatekeeper inert gas purifier) as the carrier gas, whereas for the H_2O vapor, it was first delivered into a ≈5 mL gas trap, and then delivered into the deposition chamber. Thermal oxide wafers (i.e., Si wafers with 300 nm thermally grown SiO_2 on top) were used as the substrates for studying the deposition behavior. Prior to the deposition, the wafers were treated with UV/ozone for 10 min.

Characterizations of VO_x Thin Films: Film thickness was measured by X-ray reflectometry (Bruker, D8 Advance). RBS was employed to determine the stoichiometry of the VO_x films deposited on glassy carbon substrates. The RBS experiments were performed in the Heavy Ion Institute at Peking University, using 2.022 MeV helium ions as the incident ions and collecting the back-scattered signals at the scattering angle of 165°. XPS (Thermo Scientific, Escalab 250Xi) was used to analyze the chemical composition of the deposited films. AFM (Bruker, MultiMode 8) and SEM (Zeiss, SUPRA55) were used to examine the surface morphology and the film conformality, respectively.

Fabrication of OFET Devices: OFETs were fabricated with bottom-gate/top-contact configuration on SiO_2/p^+-Si (100) substrates, where the p^+-Si and the thermally grown SiO_2 (250 nm or 300 nm) served as the gate and the dielectric, respectively. The SiO_2/Si substrates were first sequentially ultrasonicated in acetone, isopropanol, and deionized water for 10 min each, and then treated with UV/ozone for 15 min. The SiO_2/Si substrates were then immersed in 0.1 mol L^{-1} octyltrichlorosilane (OTS) in toluene for 15 min at 60 °C. The OTS-treated substrates were immediately transferred into the vacuum chamber (base pressure 2×10^{-4} Pa) for the thermal evaporation of ≈70 nm pentacene or BOPAnt as the organic semiconducting layer. The evaporation rate was maintained at 0.3–0.5 Å s^{-1}. On top of the organic layer (pentacene or BOPAnt), an ultrathin VO_x layer was deposited by the ALD process as above. The total cycles for ALD VO_x were systematically varied, in order to study the thickness dependence of VO_x for the device performance. After the ALD of VO_x, ≈50 nm of source/drain contact metal (Cu or Au) was finally evaporated through a shadow mask. The channel length and width of the OFET devices were 100 μm and 1000 μm, respectively.

Characterizations of OFET Devices: Output and transfer characteristics of the OFET devices were measured in dark, by Keithley 4200-SCS semiconductor parameter analyzer equipped with a standard probe station. To study the device shelf lifetime, the fabricated OFET devices were stored in a dark box at room temperature with 25% humidity.

Supporting Information

Supporting Information is available from the Wiley Online Library or from the author.

Acknowledgements

This work was financially supported by NSFC (Grant Nos. 51302007 and 51373075), Guangdong Natural Science Funds for Distinguished Young Scholar (Grant No. 2015A030306036), National Basic Research Program of China (973 Program, No. 2015CB932200), Shenzhen Science and Technology Innovation Committee (Grant Nos. JCYJ20140417144423201, KQCX20150327093155293, and ZDSYS20140509094114164), and Guangdong Key Research Project (2015B090914002).

Received: January 28, 2016
Revised: March 3, 2016
Published online: April 18, 2016

[1] H. Klauk, *Chem. Soc. Rev.* **2010**, *39*, 2643.
[2] H. E. A. Huitema, G. H. Gelinck, J. van der Putten, K. E. Kuijk, C. M. Hart, E. Cantatore, P. T. Herwig, A. van Breemen, D. M. de Leeuw, *Nature* **2001**, *414*, 599.

© 2016 WILEY-VCH Verlag GmbH & Co. KGaA, Weinheim

[3] P. F. Baude, D. A. Ender, M. A. Haase, T. W. Kelley, D. V. Muyres, S. D. Theiss, *Appl. Phys. Lett.* **2003**, *82*, 3964.
[4] T. Someya, T. Sekitani, S. Iba, Y. Kato, H. Kawaguchi, T. Sakurai, *Proc. Natl. Acad. Sci. USA* **2004**, *101*, 9966.
[5] B. Crone, A. Dodabalapur, Y. Y. Lin, R. W. Filas, Z. Bao, A. LaDuca, R. Sarpeshkar, H. E. Katz, W. Li, *Nature* **2000**, *403*, 521.
[6] H. Klauk, U. Zschieschang, J. Pflaum, M. Halik, *Nature* **2007**, *445*, 745.
[7] C.-A. Di, Y. Liu, G. Yu, D. Zhu, *Acc. Chem. Res.* **2009**, *42*, 1573.
[8] M. Marinkovic, D. Belaineh, V. Wagner, D. Knipp, *Adv. Mater.* **2012**, *24*, 4005.
[9] D. Natali, M. Caironi, *Adv. Mater.* **2012**, *24*, 1357.
[10] S.-W. Rhee, D.-J. Yun, *J. Mater. Chem.* **2008**, *18*, 5437.
[11] F. Amy, C. Chan, A. Kahn, *Org. Electron.* **2005**, *6*, 85.
[12] M. Kano, T. Minari, K. Tsukagoshi, *Appl. Phys. Lett.* **2009**, *94*, 143304.
[13] A. Kumatani, Y. Li, P. Darmawan, T. Minari, K. Tsukagoshi, *Sci. Rep.* **2013**, *3*, 1026.
[14] P. Darmawan, T. Minari, A. Kumatani, Y. Li, C. Liu, K. Tsukagoshi, *Appl. Phys. Lett.* **2012**, *100*, 013303.
[15] M. T. Greiner, M. G. Helander, W. M. Tang, Z. B. Wang, J. Qiu, Z. H. Lu, *Nat. Mater.* **2012**, *11*, 76.
[16] J. Meyer, K. Zilberberg, T. Riedl, A. Kahn, *J. Appl. Phys.* **2011**, *110*, 033710.
[17] Q. Chen, B. J. Worfolk, T. C. Hauger, U. Al-Atar, K. D. Harris, J. M. Buriak, *ACS Appl. Mater. Interfaces* **2011**, *3*, 3962.
[18] D. X. Long, K.-J. Baeg, Y. Xu, S.-J. Kang, M.-G. Kim, G.-W. Lee, Y.-Y. Noh, *Adv. Funct. Mater.* **2014**, *24*, 6484.
[19] K. J. Baeg, G. T. Bae, Y. Y. Noh, *ACS Appl. Mater. Interfaces* **2013**, *5*, 5804.
[20] D. Barreca, L. Armelao, F. Caccavale, V. Di Noto, A. Gregori, G. A. Rizzi, E. Tondello, *Chem. Mater.* **2000**, *12*, 98.
[21] X. Chen, E. Pomerantseva, P. Banerjee, K. Gregorczyk, R. Ghodssi, G. Rubloff, *Chem. Mater.* **2012**, *24*, 1255.
[22] C. V. Ramana, O. M. Hussain, B. S. Naidu, P. J. Reddy, *Thin Solid Films* **1997**, *305*, 219.
[23] L.-J. Meng, R. A. Silva, H.-N. Cui, V. Teixeira, M. P. dos Santos, Z. Xu, *Thin Solid Films* **2006**, *515*, 195.
[24] C. V. Ramana, R. J. Smith, O. M. Hussain, C. C. Chusuei, C. M. Julien, *Chem. Mater.* **2005**, *17*, 1213.
[25] S. Passerini, D. Chang, X. Chu, D. B. Le, W. Smyrl, *Chem. Mater.* **1995**, *7*, 780.
[26] S. Schiefer, M. Huth, A. Dobrinevski, B. Nickel, *J. Am. Chem. Soc.* **2007**, *129*, 10316.
[27] S. M. George, *Chem. Rev.* **2010**, *110*, 111.
[28] M. Leskela, M. Ritala, *Thin Solid Films* **2002**, *409*, 138.
[29] M.-G. Willinger, G. Neri, E. Rauwel, A. Bonavita, G. Micali, N. Pinna, *Nano Lett.* **2008**, *8*, 4201.
[30] X. Sun, C. Zhou, M. Xie, T. Hu, H. Sun, G. Xin, G. Wang, S. M. George, J. Lian, *Chem. Commun.* **2014**, *50*, 10703.
[31] T. Blanquart, J. Niinistö, M. Gavagnin, V. Longo, M. Heikkilä, E. Puukilainen, V. R. Pallem, C. Dussarrat, M. Ritala, M. Leskelä, *RSC Adv.* **2013**, *3*, 1179.
[32] E. Østreng, O. Nilsen, H. Fjellvåg, *J. Phys. Chem. C* **2012**, *116*, 19444.
[33] J. Musschoot, D. Deduytsche, H. Poelman, J. Haemers, R. L. Van Meirhaeghe, S. Van den Berghe, C. Detavernier, *J. Electrochem. Soc.* **2009**, *156*, P122.
[34] P. A. Premkumar, M. Toeller, I. P. Radu, C. Adelmann, M. Schaekers, J. Meersschaut, T. Conard, S. V. Elshocht, *ECS J. Solid State Sci. Technol.* **2012**, *1*, P169.
[35] G. Rampelberg, M. Schaekers, K. Martens, Q. Xie, D. Deduytsche, B. De Schutter, N. Blasco, J. Kittl, C. Detavernier, *Appl. Phys. Lett.* **2011**, *98*, 162902.
[36] A. Benayad, H. Martinez, A. Gies, B. Pecquenard, A. Levasseur, D. Gonbeau, *J. Electron Spectrosc. Relat. Phenom.* **2006**, *150*, 1.
[37] L. Yan, Y. Zhao, H. Yu, Z. Hu, Y. He, A. Li, O. Goto, C. Yan, T. Chen, R. Chen, Y.-L. Loo, D. F. Perepichka, H. Meng, W. Huang, unpublished.
[38] C. Liu, Y. Xu, Y.-Y. Noh, *Mater. Today* **2015**, *18*, 79.
[39] Y. Xu, T. Minari, K. Tsukagoshi, J. A. Chroboczek, G. Ghibaudo, *J. Appl. Phys.* **2010**, *107*, 114507.
[40] J. E. Northrup, M. L. Chabinyc, *Phys. Rev. B* **2003**, *68*, 041202.
[41] A. Risteska, J. Bedolla, J. E. Northrup, W. Bergholz, V. Wagner, D. Knipp, *Adv. Electron. Mater.* **2016**, *2*, 1500179.
[42] W. Melitz, J. Shen, A. C. Kummel, S. Lee, *Surf. Sci. Rep.* **2011**, *66*, 1.
[43] H. Ishii, K. Sugiyama, E. Ito, K. Seki, *Adv. Mater.* **1999**, *11*, 605.
[44] M. D. Groner, S. M. George, R. S. McLean, P. F. Carcia, *Appl. Phys. Lett.* **2006**, *88*, 051907.
[45] Y. Yong-Qiang, D. Yu, *J. Phys. Chem. C* **2014**, *118*, 18783.
[46] J.-S. Park, H. Chae, H. K. Chung, S. I. Lee, *Semicond. Sci. Technol.* **2011**, *26*, 034001.

© 2016 WILEY-VCH Verlag GmbH & Co. KGaA, Weinheim